

## XAS Study of Iron and Arsenic Speciation during Fe(II) Oxidation in the Presence of As(III)

S. THORAL,<sup>†</sup> J. ROSE,<sup>\*,†</sup> J. M. GARNIER,<sup>†</sup>  
A. VAN GEEN,<sup>‡</sup> P. REFAIT,<sup>§</sup>  
A. TRAVERSE,<sup>||</sup> E. FONDA,<sup>⊥</sup>  
D. NAHON,<sup>†</sup> AND J. Y. BOTTERO<sup>†</sup>

CEREGE UMR 6635 CNRS-Université Paul Cézanne  
Aix-Marseille III, IFR PMSE 112, Europpôle Méditerranéen de  
l'Arbois, 13545 Aix-en-Provence, France, LDEO Columbia  
University, Palisades, New York 10964, LEMMA, EA 3167,  
Université de La Rochelle, Avenue M. Crépeau, 17042 La  
Rochelle, France, LURE, Université Paris-Sud, Orsay, France,  
and Synchrotron SOLEIL, l'Orme des Merisiers, Saint-Aubin,  
91192 Gif-sur-Yvette, France

The speciation of As and Fe was studied during the oxidation of Fe(II)–As(III) solutions by combining XAS analysis at both the Fe and As K-edges. Fe(II) and As(III) were first hydrolyzed to pH 7 under anoxic conditions; the precipitate was then allowed to oxidize in ambient air for 33 h under vigorous stirring. EXAFS analysis at the As K-edge shows clear evidence of formation of inner-sphere complexes between As(III) and Fe(II), i.e., before any oxidation. Inner-sphere complexes were also observed when Fe became sufficiently oxidized, in the form of edge-sharing and double-corner linkages between As<sup>III</sup>O<sub>3</sub> pyramids and Fe<sup>III</sup>O<sub>6</sub> octahedra. XAS analyses at the Fe K-edge reveal that the presence of As(III) in the solution limits the polymerization of Fe(II) and the formation of green rust and inhibits the formation of goethite and lepidocrocite. Indeed, As(III) accelerates the Fe(II) oxidation kinetics and leads to the formation of nanosized Fe–As subunits of amorphous aggregates. These observations, rather than a presumed weaker affinity of As(III) for iron oxyhydroxides, might explain why As(III) is more difficult to remove than As(V) by aerating reducing groundwater.

### Introduction

The recent finding that groundwaters from large areas of Bangladesh and West Bengal, India, are enriched in As, a highly toxic element, has increased the number of studies dealing with the mobility of arsenic in reducing aquifers. The mobility of As(III) was commonly considered to be greater than that of As(V) (1–2), but the universality of this notion has recently been successfully challenged (3). It remains true that iron oxyhydroxide phases probably play a key but complex role in controlling the mobility and fate of arsenic in groundwater (e.g., 4–7). The sorption of As onto iron(III) oxyhydroxides has been well established quantitatively as

well as structurally down to the molecular scale using extended X-ray absorption fine structure (EXAFS) spectroscopy. As(V) forms inner-sphere bidentate binuclear complexes at the Fe<sup>III</sup>OOH surface (8–12) and at the green-rust (GR) [iron(II/III) oxyhydroxides] surface (13). There is also evidence of inner-sphere adsorption of As(III) at the Fe<sup>III</sup>OOH surface (11, 12, 14). Much less is known about the potential interactions between Fe(II) and As(III) species that might also be important in regulating dissolved As concentrations in natural waters.

In reducing Bangladesh aquifers, often associated with elevated As concentrations, there is evidence of widespread conversion of iron(III) oxyhydroxides to Fe(II) or mixed Fe(II/III) phases (5, 15). The implications of such transformations on As mobility are poorly understood, although a recent laboratory study has shown that the binding of As to magnetite [mixed Fe(II/III) phase], for instance, is about as strong as its binding to a pure iron(III) oxyhydroxide (16). The reverse process of oxidation of Fe(II) in the presence of As(III) also needs to be understood better as it applies to several types of As-removal systems that have been tested in Bangladesh (4, 12, 17). It is not clear, whether As(III) might already be linked to Fe(II) at the very first step of Fe precipitation through oxidation.

In the present study, changes in the atomic structure and the redox state of synthetic As(III)–Fe(II) precipitates during gradual oxidation over a period of 33 h were studied using X-ray absorption spectroscopy (XAS).

### Materials and Methods

**Sample Preparation.** A solution containing 0.2 M Fe(II) and 0.2 M As(III) was prepared by first adding 3.90 g of NaAsO<sub>2</sub> to 135 mL of doubly distilled water with 15 mL of 1 M HCl in a 500-mL polyethylene flask with stirring. The solution was prepared in a glovebag containing 90% N<sub>2</sub> and 10% H<sub>2</sub>; 5.96 g of FeCl<sub>2</sub>·4H<sub>2</sub>O was added after the arsenic salt had completely dissolved. The addition of HCl is needed to form Fe(II) and As(III) monomers at the onset of the titration (18, 19). The solution was hydrolyzed by increasing the pH to 7 within 20 min with aliquots of 10 M NaOH. The solution was then removed from the glovebag and allowed to oxidize in ambient air under vigorous stirring for 33 h. During this time, a constant pH was maintained through periodic additions of NaOH, and the E<sub>h</sub> of the solution was also monitored with a calibrated platinum electrode. The same procedure was followed with a standard 0.2 M Fe(II) solution that was allowed to oxidize for 15 h.

Aliquots (15 mL) of the As(III)–Fe(II) and Fe(II) solutions were sampled over the course of oxidation at four and three intervals, respectively (Table 1). Subsamples (5 mL) were filtered through 0.45- $\mu$ m syringe filters and analyzed for Fe and As quantification by inductively coupled plasma-atomic emission spectroscopy (Jobin-Yvon ULTIMA C). The measurements indicate that 4% and 7%, respectively, of the As and Fe initially in the solution remained in the solution of the Fe(II)–As(III) system (i.e., an As/Fe ratio of  $\sim$ 1). The remaining 10 mL of slurry was allowed to settle for  $\sim$ 30 min in a 25-mL polyethylene flask in a glovebag periodically purged with 90%/10% N<sub>2</sub>/H<sub>2</sub>. The concentrated precipitate was collected with a needle attached to a syringe and transferred to a variable-step cell within a hermetically sealed box for immediate XAS analysis. The box was cooled at 5 °C and flushed with N<sub>2</sub> to inhibit further oxidation.

**X-ray Absorption Spectroscopy (XAS).** Fe and As K-edge XAS spectra were recorded in transmission mode at beam line D42, DCI ring, at 1.85 GeV and 200 mA (LURE, Orsay,

\* Corresponding author phone: 33 4 42 97 15 29; fax: 33 4 42 97 15 59; e-mail: rose@cerge.fr.

<sup>†</sup> CEREGE UMR 6635 CNRS-Université Paul Cézanne Aix-Marseille III.

<sup>‡</sup> LDEO Columbia University.

<sup>§</sup> Université de La Rochelle.

<sup>||</sup> Université Paris-Sud

<sup>⊥</sup> Synchrotron SOLEIL.

**TABLE 1. Structural Parameters for Fe<sup>a</sup> Contributions Deduced from EXAFS Analysis for the Fe(II) and Fe(II)–As(III) Systems**

sampling time (min)	atomic shell	<i>R</i> (Å) (±0.02 Å)	<i>σ</i> (Å) (±0.01 Å)	<i>N</i> (±20%)	<i>χ</i> <sup>2</sup>
<b>Fe(II) System</b>					
<i>t</i> = 0	Fe–O	2.12	0.085	6.0	44
	Fe–Fe	3.25	0.078	4.3	
<i>t</i> = 200	Fe–O	2.09	0.104	6.0	33
	Fe–Fe	3.20	0.074	4.80	
<i>t</i> = 800	Fe–O	2.09	0.105	6.0	66
	Fe–Fe	3.20	0.074	5.8	
<b>Fe(II)–As(III) System</b>					
<i>t</i> = 0	Fe–O	2.11	0.092	6.0	20.8
	Fe–Fe	3.24	0.084	3.8	
<i>t</i> = 200	Fe–O	2.08	0.120	6.0	31.8
	Fe–Fe	3.21	0.085	3.0	
<i>t</i> = 800	Fe–O	2.00	0.112	6.0	15
	Fe–Fe	3.14	0.107	2.3	
	Fe–As	3.37	0.063	1.3	
	Fe–Fe	3.60	0.059	0.7	
<i>t</i> = 1500	Fe–O	1.99	0.107	6.0	16
	Fe–Fe	3.06	0.098	2.1	
	Fe–As	3.39	0.062	0.9	

<sup>a</sup> Backscatterer in the first and second coordination spheres.

France). A Si(111) monochromator was used. XAS spectra were acquired in the –100 to +1000 eV energy range relative to the K-edges of Fe and As. The preedge portion of X-ray absorption near-edge structure (XANES) was extracted from region extended from 7050 to 7100 eV and from 11830 to 11850 eV for the Fe and As K-edges, respectively. The absorption jump of the XANES spectra was normalized by fitting the photoelectric background above the absorption edge with a second-order polynomial function.

EXAFS (extended X-ray absorption fine structure) data were reduced (20) following a previously described procedure (21):  $k^3\chi(k)$  spectra ( $k$  = wave vector) were Fourier transformed from  $k$  to  $R$  space using a Kaiser apodization window with  $\tau = 2.5$  (22). Fourier transformation of the  $\chi(k)$  function leads to a radial distribution function (RDF) for which the peak positions correspond to the interatomic distances within the sample. These RDFs are uncorrected for phase shifts so that the positions are slightly shifted by  $\Delta R \approx -0.3$  Å from the actual distances. Raw EXAFS spectra were least-squares fitted with a theoretical function to determine the structural and chemical parameters  $R_j$  (distances between neighbors) and  $N_j$  (number of neighbors), as well as the nature of atomic neighbors in the  $j$ th shell around the central atom. The limit on the number of independent parameters [ $N_{\text{ind}} = (2\Delta k\Delta R)/\pi$ ] was never exceeded during modeling. Estimated errors for distances and coordination numbers are  $\pm 0.02$  Å and  $\pm 20\%$ , respectively. The best fit to the data was determined by minimizing the normalized square difference function, which depends on the number of independent parameters  $N_{\text{ind}}$ , the number of fit parameters, and the absolute error of the data.

Amplitude ( $F_{i-j}$ ) and phase shift ( $\phi_{i-j}$ ) functions for the different  $i-j$  pairs are required to fit EXAFS spectra by theoretical functions. These functions were defined using the single-scattering, curved-wave FEFF model (23). The validity of the theoretical functions was ascertained with pure and well-crystallized references: andradite (Ca<sub>3</sub>Fe<sub>2</sub>Si<sub>3</sub>O<sub>12</sub>) and Fe(OH)<sub>2</sub> for the Fe–O wave, lepidocrocite ( $\gamma$ -FeOOH) and Fe(OH)<sub>2</sub> for the Fe–Fe wave, scorodite (FeAsO<sub>4</sub>·7H<sub>2</sub>O) for the Fe–As and As–Fe waves, and scorodite (FeAsO<sub>4</sub>·7H<sub>2</sub>O) and arsenolite (As<sub>2</sub>O<sub>3</sub>) for the As–O wave. These references were used to determine the electron mean free path function [ $\lambda(k) = 2k/\Gamma$ ] and the energy offset ( $\Delta E_0$ ) of each  $i-j$  pair, which was then kept fixed to fit unknown samples.

## Results

**XANES Data.** XANES spectra at the Fe K-edge are sensitive to the oxidation state of Fe as well as its local structure. The only accurate method for determining the oxidation state is based on the analysis of the preedge peak (24–26). Unfortunately, in our case, the resolution of the beam line did not allow us to accurately determine the shape and position of the preedge for such a determination.

Nevertheless, the spectra for the time series of samples (Figure 1A) can be compared to those of pure reference compounds, Fe<sup>II</sup>(OH)<sub>2</sub> and ferrihydrite [Fe(III)]. The increase in energy of the maximum of the white line occurs more rapidly for the Fe(II)–As(III) system than for the Fe(II) system. This indicates that the presence of As(III) has a strong effect on the evolution of the oxidation state and/or the Fe local order.

Comparison of the As XANES spectra of the time-series samples with As XANES spectra of pure reference compounds (As<sup>III</sup><sub>2</sub>O<sub>3</sub> and As<sup>V</sup><sub>2</sub>O<sub>5</sub>) indicates that As remained in the +III oxidation state throughout the experiments (Figure 1B).

**EXAFS Data.** Comparison of experimental Fe  $\chi(k)$  spectra indicates that the atomic environment of Fe was strongly modified by the presence of As(III) (Figure 2A). The maximum of the oscillation centered at 6 Å<sup>-1</sup> for both systems at  $t = 0$  min, for instance, increases strongly in the case of the Fe(II)–As(III) system over time, whereas it remains almost at the same position for the Fe(II) system. The Fe radial distribution functions (RDFs) consist of two main peaks up to 4 Å (Figure 2B). The first peak for both systems is due exclusively to Fe–O bonds. At  $t = 0$  and 200 min, the average Fe–O distance for both systems is greater than 2.08 Å (Table 1). In the case of the Fe(II) system, the Fe–O distance remains in the same range at  $t = 800$  min, whereas for the Fe(II)–As(III) system, the distance decreases significantly (2.00 Å). An even lower Fe–O distance is observed at  $t = 1500$  min.

The second peak of the RDF corresponds to contributions from Fe–Fe and/or Fe–As. In the case of the Fe(II) system, the intensity of the second peak increases during oxidation, whereas a decrease and modification of the shape of the second peak is observed for the Fe(II)–As(III) system (Figure 2B). For the Fe(II) system, the second coordination sphere consists of one Fe shell with Fe–Fe interatomic distances varying from 3.20 to 3.25 Å (Table 1). In the case of the Fe(II)–As(III) system, the second coordination sphere consists of Fe–Fe (3.06–3.60 Å) and Fe–As (3.37–3.39 Å) interatomic distances.

The similarity between the experimental As  $\chi(k)$  spectra of all four samples indicates that the As atomic environment did not change dramatically over time (Figure 2C). The fits of the raw EXAFS spectra yielded a remarkably constant As–O distance and coordination number over the course of oxidation (Table 2). These parameters are identical to those of the arsenolite As<sup>III</sup><sub>2</sub>O<sub>3</sub> and confirm the evidence from the As XANES data that As remained in the +III oxidation state throughout the experiment.

The second shell between  $R + \Delta R = 2.4$  and  $R + \Delta R = 3.4$  Å in the RDF (distances not corrected for phase shift) corresponds mainly to As–Fe atomic pairs (Figure 2D). It consists of a single peak at 3.30 Å (Table 2) for the two most reduced samples at  $t = 0$  and 200 min that broadened somewhat over time. Another iron shell at 3.67 Å (real distance) can be added at  $t = 200$  min to obtain a better fit. In addition, the As RDFs show another fairly well separated peak at  $R + \Delta R = 2.5$ – $2.6$  Å for samples at  $t = 800$  and 1500 min (Figure 2D). For these samples, a shell of Fe at 2.81 and 2.80 Å is required to obtain a reasonable fit.

## Discussion

**Structural Relation between As and Fe Polyhedra.** The structure of Fe and Fe–As colloids can be determined from

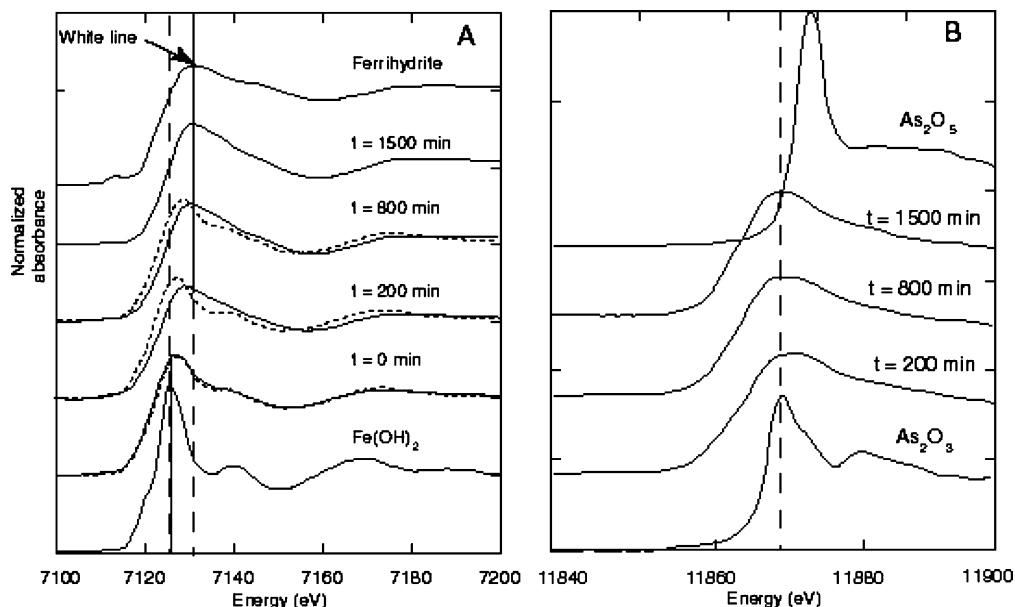


FIGURE 1. (A) Fe K-edge XANES spectra for samples of the Fe(II)–As(III) (solid lines) and Fe(II) (dotted lines) systems and for the reference compounds  $\text{Fe}^{\text{II}}(\text{OH})_2$  and ferrihydrite [ $\text{Fe}^{\text{III}}$ ] and (B) As K-edge XANES spectra for samples of the Fe(II)–As(III) system.

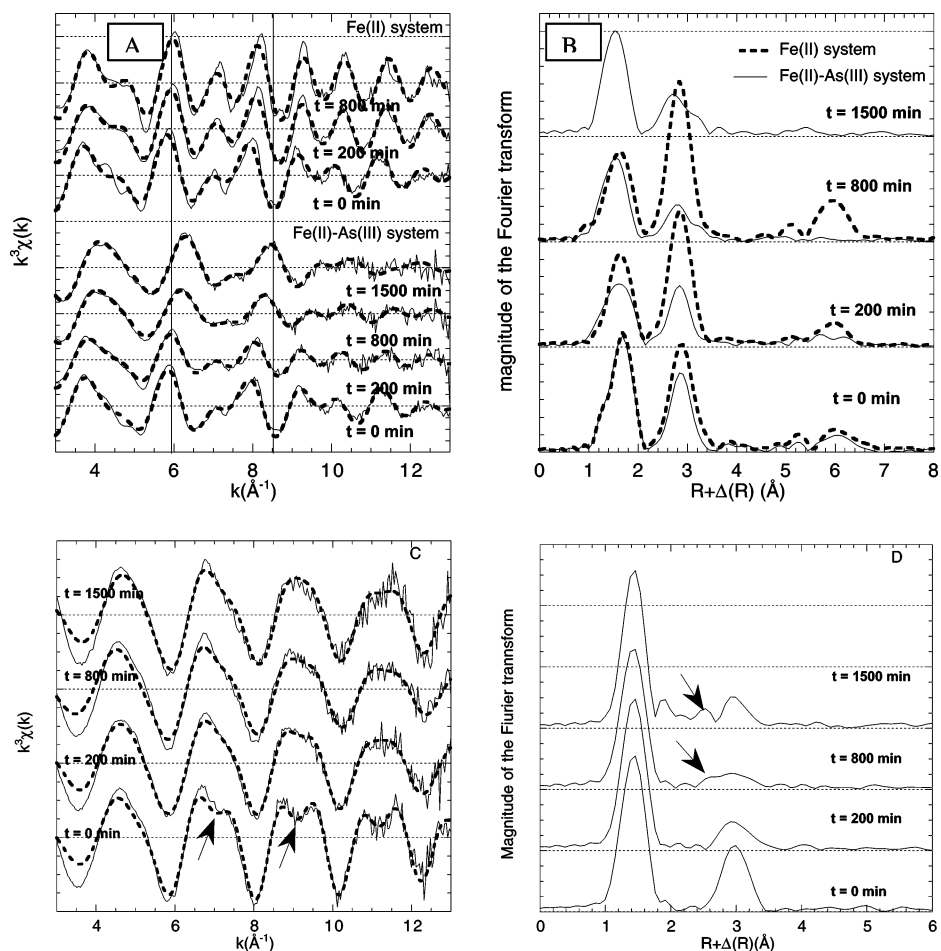


FIGURE 2. Fe EXAFS spectra for the Fe(II)–As(III) system at four stages of oxidation and for the Fe(II) system at three stages of oxidation: (A)  $k^3$ -weighted  $\chi(k)$  experimental functions (solid lines) compared to the calculated curves (dotted lines) and (B) their corresponding radial distribution functions (RDFs) uncorrected for phase shifts. As K-edge EXAFS spectra for the Fe(II)–As(III) system at four stages of oxidation: (C)  $k^3$ -weighted  $\chi(k)$  experimental functions (solid lines) compared to the calculated curves (dotted lines) and (D) their corresponding radial distribution functions (RDFs) uncorrected for phase shifts. Arrows identify the appearance of a second peak in the RDF through oxidation.

EXAFS data using the polyhedral approach (27, 28). At the Fe K-edge, the Fe–Fe distance at 3.25 Å is consistent with

$\text{Fe}^{\text{II}}\text{O}_6$  octahedra sharing edges, as in the model compound  $\text{Fe}^{\text{II}}(\text{OH})_2$ . The 3.20 Å Fe–Fe distance is typical of green-rust

**TABLE 2. Structural Parameters for As<sup>a</sup> Contributions Deduced from EXAFS Analysis for the Fe(II)–As(III) System**

sampling time (min)	atomic shell	$R$ (Å) (±0.02 Å)	$\sigma$ (Å) (±0.01 Å)	N (±20%)	$\chi^2$
$t = 0$	As–O	1.77	0.059	3.0	66
	As–Fe	3.30	0.058	2.2	
$t = 200$	As–O	1.77	0.056	3.0	41
	As–Fe	3.30	0.070	1.3	
	As–Fe	3.67	0.09	0.5	
$t = 800$	As–O	1.76	0.060	3.0	132
	As–Fe	2.81	0.080	0.2	
	As–Fe	3.30	0.08	1.5	
	As–Fe	3.30	0.08	1.5	
$t = 1500$	As–O	1.77	0.050	3.0	65
	As–Fe	2.80	0.085	0.5	
	As–Fe	3.31	0.056	1.0	

<sup>a</sup> Backscatterer in the first and second coordination spheres.

minerals (29). This distance could reflect Fe<sup>II</sup>O<sub>6</sub> and Fe<sup>III</sup>O<sub>6</sub> octahedra sharing edges (30).

For the Fe<sup>II</sup>–As<sup>III</sup> system, the Fe–Fe interatomic distances [3.24–3.06 Å (Table 1)] also indicate edge sharing between FeO<sub>6</sub> octahedra. The interatomic distance of 3.06 Å corresponds to edge sharing between Fe<sup>III</sup>O<sub>6</sub> octahedra (19, 27, 28). For the two most oxidized samples, such a model produces Fe–As<sup>III</sup> interatomic distances of 3.37 and 3.39 Å, respectively. These distances can be attributed to double-corner linkages between Fe<sup>III</sup>O<sub>6</sub> octahedra and As<sup>III</sup>O<sub>3</sub> pyramids, as previously described by Manning et al. (14) and Farquhar et al. (11). For  $t = 800$  min, another Fe–Fe bond had to be included that consists of FeO<sub>6</sub> octahedra sharing two corners (0.7 Fe at 3.60 Å) (Table 2).

At the As K-edge, the As–Fe interatomic distance of 3.30–3.31 Å observed in each sample is very close to the average As<sup>III</sup>–Fe<sup>III</sup> interatomic distances of 3.31 Å (11) and 3.38 Å (14) associated with binuclear bridging complexes in the case of As(III) adsorbed on goethite. Because data from the Fe K-edge indicate that at least the two most reduced samples from the Fe(II)–As(III) system are primarily composed of Fe(II) (see below), this suggests that the As–Fe interatomic distance of 3.30–3.01 Å is associated with Fe<sup>II</sup>O<sub>6</sub> octahedra and As<sup>III</sup>O<sub>3</sub> pyramids sharing two corners. There are no reports of such a type of complex in the literature, and thus, no typical As(III)–Fe(II) interatomic distances available for comparison. The longest As–Fe distance (3.67 Å, Table 2) is characteristic of a linear monodentate complex described in the cases of both As(V) (10) ( $R_{\text{As}^{\text{V}}-\text{Fe}^{\text{III}}} = 3.57$  Å) and As(III) (14) ( $R_{\text{As}^{\text{III}}-\text{Fe}^{\text{III}}} = 3.59$ –3.60 Å) adsorbed on goethite. The last distance at 2.80–2.81 Å found for the two most oxidized samples is, in the case of As(III), undoubtedly indicative of an As(III)–Fe edge-sharing complex. In the case of As(V), the As(V)–Fe distance of 2.8–2.9 Å is controversial. Various authors have indicated that such distances correspond to edge sharing between As and Fe polyhedra (8, 11, 13). However, Sherman and Randall (31) showed that the RDF peak at  $R + \Delta R = 2.5$ –2.6 Å is not due to As(V)–Fe backscatter but results from multiple scattering of the photoelectron involving O–O pairs within the AsO<sub>4</sub> tetrahedron (As–O–O path = 2.8–2.9 Å). In the case of the As(III)–O<sub>3</sub> tetrahedron, the shortest As–O–O multiple-scattering path appears at 3.05 Å, and the amplitude of the signal is low. Therefore, all of our attempts to include multiple scattering in the calculation failed, and the As<sup>III</sup>–Fe contribution was necessary to reproduce the experimental spectra.

**Presence of As(III) around Fe(II): Need for a Multiple-Edge XAS Analysis.** Data from the As K-edge reveal the presence of linkages between As<sup>III</sup>O<sub>3</sub> and FeO<sub>6</sub> (Table 2) for all of the samples from the Fe(II)–As(III) system. One might therefore expect that data from the Fe K-edge would indicate the presence of neighboring arsenic. Unfortunately, this is

not the case for the two most reduced samples (Table 2). Fe back-Fourier transforms of the second peak of the most reduced samples do not show any beat nodes (data not shown) and, thus, no evidence of such Fe–As contributions in addition to the Fe–Fe contributions. This is attributed to phase opposition (cancellation effect) throughout the  $k$  range of Fe–Fe waves at 3.24–3.21 Å with Fe–As waves at 3.33–3.32 Å (Figure 3A). Hence, it is difficult to detect As structurally associated with Fe from the modeling at the Fe K-edge.

Examples detailed in Figure 3 illustrate the difficulty of determining the presence of As at the Fe K-edge and the importance of a multiple XAS K-edge analysis.

**Effect of As(III) Binding on Fe(II) Oxidation Kinetic.** The contrasting evolution of  $E_h$  during the two experiments could potentially reflect the faster Fe(II) oxidation in the presence of As(III) (Supporting Information), but this is difficult to confirm with the XANES data. Indeed, a decrease of iron(II) hydroxide crystallinity could, for instance, also lead to a positive shift (Supporting Information), but such a shift in energy is generally low (~1 eV) in the case of modification of the crystallinity of the particles. On the other hand, the oxidation of Fe(II) to Fe(III) for well-crystallized iron oxides leads to a more significant shift of the white line (>4 eV, Supporting Information). It seems, therefore, that the 3.3 eV increase of the position of the maximum of the white line for the Fe(II)–As(III) system (Figure 2) cannot be due only to the evolution of the local order but must also be due to the evolution of the redox state.

Changes in the average Fe–O distance over the course of the experiment provide independent evidence of the oxidation of Fe. Indeed, the average Fe–O distance is in the 2.9–3.05 Å range in the case of Fe(III), whereas in the case of Fe(II) systems, the average distance is in the 2.1–2.16 Å range (30, 36). Some ambiguity remains, however, because Fe(III)–O distances can reach 2.10 Å by distortion of Fe octahedra in amorphous systems.

Fe–Fe distances are also modified by oxidation of Fe; data drawn from various studies of pure Fe(II) and Fe(III) samples (27, 30, 32–38) suggest a correlation between Fe–O and Fe–Fe distances (Figure 4). In the case of Fe<sup>II</sup>(OH)<sub>2</sub>, the average Fe–O and Fe–Fe(edge) distances are 2.121 (±0.012) and 3.263 (±0.014) Å, respectively, whereas for Fe<sup>III</sup>OOH, the average distances are 1.991 (±0.012) and 3.061 (±0.036) Å for the Fe–O and Fe–Fe(edge) contributions, respectively. Fe–O and Fe–Fe distances corresponding to the initial state of the Fe(II) system ( $t = 0$ ) fit the iron(II) hydroxide domain defined by the previous studies (Figure 4). At  $t = 200$  and 800 min, the points are very close to the green-rust zone. Between  $t = 0$  and  $t = 200$  min, the evolution of the Fe(II)–As(III) system is quite similar. At  $t = 800$  min, however, the Fe–O and Fe–Fe distances approach the Fe<sup>III</sup>OOH domain (Figure 4). When combined, the individually ambiguous  $E_h$  and XANES data therefore strongly suggest that the oxidation of Fe(II) is considerably faster in the presence of As(III).

This result is surprising. Indeed, Benali et al. (39) have shown that the sorption of anions such as PO<sub>4</sub><sup>3-</sup> at the GR surface can decrease the Fe(II) oxidation rate. In the present case, the effect of As anions on the Fe(II) oxidation appears to be reversed. The mechanisms involved are unclear but, as discussed below, might be related to a decrease in particle size (or the size of subunits forming large aggregates).

**Effects of As(III) Binding on Fe Particle Growth, Structure, and Size.** On the basis of structural parameters determined by EXAFS, the evolution of the particle structure and size during the experiments (and/or the structure of the subunits constituting a large aggregate) can be hypothesized. This is because the coordination number  $N_{\text{Fe}}$  is proportional to the size of the particles or the subunits (37, 40–42). In the case of large particles with the Fe(OH)<sub>2</sub> or the GR structure, each iron octahedron is surrounded by six other edge-sharing

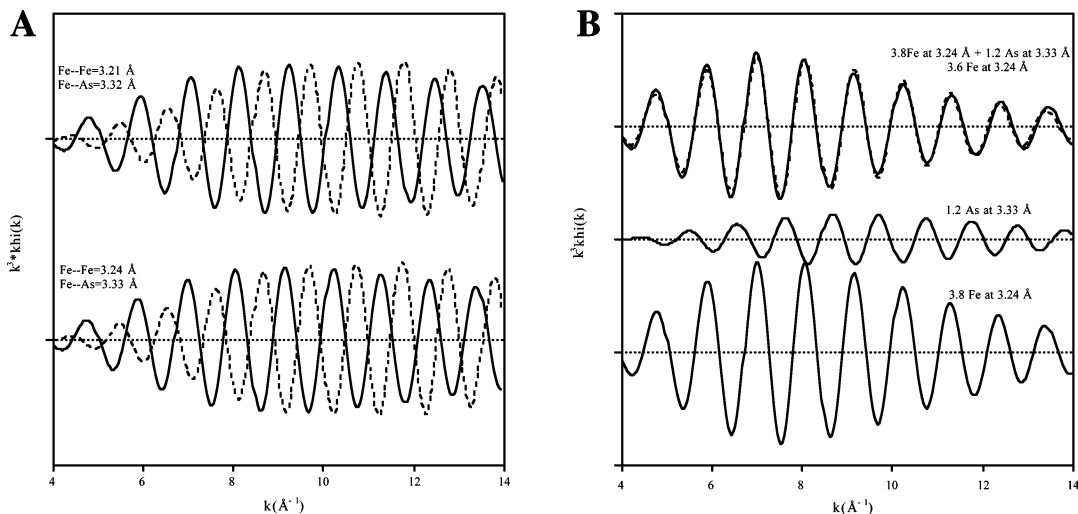


**FIGURE 3.** (A) Superimposition of (bottom) calculated waves for Fe–Fe = 3.24 Å,  $N = 1$ ,  $-\Delta E = 2.5$  (solid lines) and Fe–As = 3.33 Å,  $N = 1$ ,  $-\Delta E = 2.5$  (dotted lines) and (top) calculated waves for Fe–Fe = 3.21 Å,  $N = 1$ ,  $-\Delta E = 2.5$  (solid lines) and Fe–As = 3.32 Å,  $N = 1$ ,  $-\Delta E = 2.5$  (dotted lines). (B) (Bottom) Calculated Fe–Fe wave ( $N_{\text{Fe-Fe}} = 3.8$ ,  $R_{\text{Fe-Fe}} = 3.24$  Å,  $\sigma = 0.08$ ). (Middle) Calculated Fe–As wave ( $N_{\text{Fe-As}} = 1.2$ ,  $R_{\text{Fe-As}} = 3.33$  Å,  $\sigma = 0.08$ ). (Top) Sum of the two waves (Fe–Fe and Fe–As) as an experimental signal (solid lines) superimposed together with the calculated spectrum using one Fe–Fe contribution (dotted lines; resulting parameters:  $N_{\text{Fe-Fe}} = 3.6$ ,  $R_{\text{Fe-Fe}} = 3.24$  Å,  $\sigma = 0.08$ ). The Fe–As contribution is not detected by modeling.

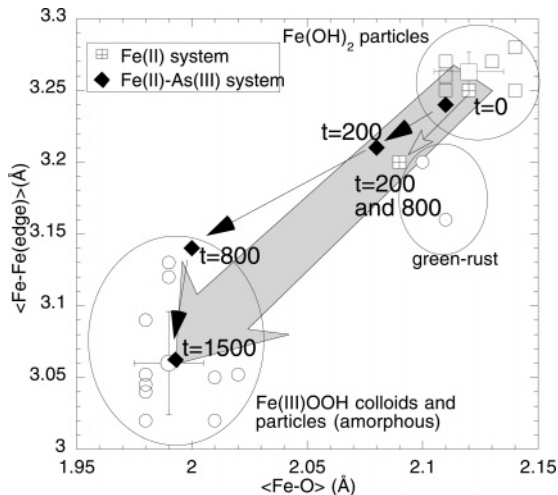


**FIGURE 4.** Average Fe–O distances plotted as a function of average Fe–Fe distances (only edge sharing) for pure iron(II) and iron(III) oxyhydroxide particles.

octahedra (i.e.,  $N_{\text{Fe}}^{\text{theo}} = 6$ ). For smaller particles, the proportion of border octahedra that are linked to fewer than six irons increases leading to a decrease in  $N_{\text{Fe}}^{\text{theo}}$  (Supporting Information). The main limitation of this calculation is that the uncertainty of  $N$  is high ( $\pm 20\%$ ).

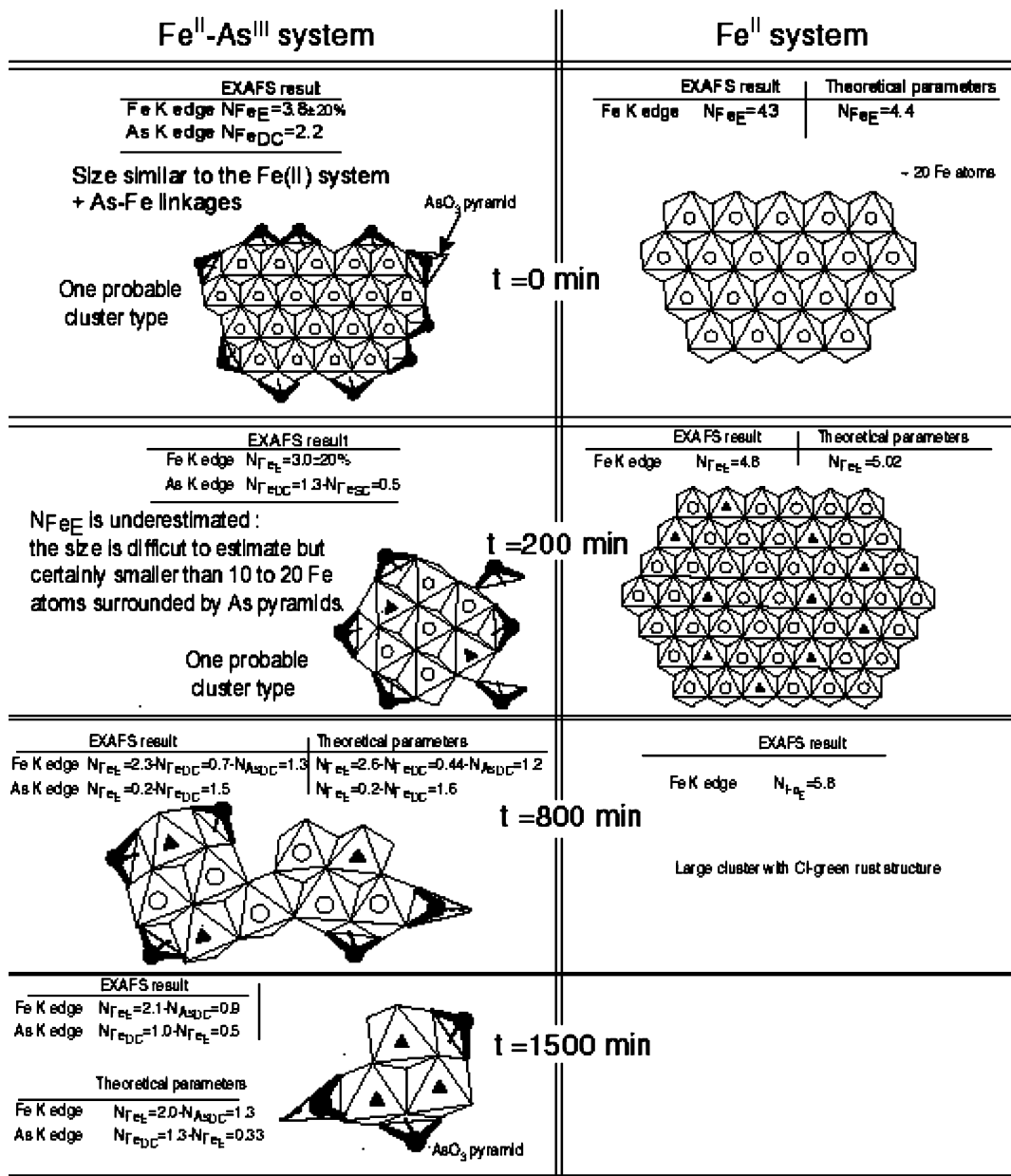
In the case of the pure Fe(II) system under anoxic conditions, it has been shown that the hydrolysis of an iron(II) chloride solution leads to the formation of Fe(OH)<sub>2</sub> and follows various steps (30, 43). Doelsch et al. (30) showed that hydrolysis, condensation, and polymerization of Fe(II) under anoxic conditions involve first the formation of small clusters with a planar structure ( $0.1 \leq R = [\text{OH}]/[\text{Fe}] < 1$ , i.e.,  $6.5 \leq \text{pH} < 7.6$ ) and then the formation of intermediate polycations whose local structure is that of Fe<sup>II</sup>(OH)<sub>2</sub> ( $R \geq 1$ , i.e.,  $\text{pH} \geq 7.6$ ). In the present study, data for the Fe(II) system at  $t = 0$  (i.e., after the hydrolysis under anoxic conditions) also indicate the formation of planar primary clusters whose local structure is that of Fe<sup>II</sup>(OH)<sub>2</sub>. On the basis of this reasoning, we can propose the formation of clusters with a mean number of 20 octahedra for the Fe(II) system (Figure 5). The structure of the cluster for  $t = 0$  is not unique, and various clusters can

result in a same theoretical coordination number. Therefore, the cluster is given only to illustrate the structure and roughly quantify the size of the polymer. In the case of the Fe(II)–As(III) system,  $N_{\text{Fe}}$  is in the same range and reflects a similar cluster size within  $\pm 20\%$ . This observation suggests that the effect of As(III) on the polymerization of Fe(II) during hydrolysis under anoxic conditions is limited.

Fe EXAFS results show that the effect of As(III) on the structure of the precipitates through Fe(II) oxidation is more significant than that through Fe(II) polymerization under anoxic conditions. The number of edge-sharing neighbors ( $N_{\text{FeE}}$ ) increases from 4.3 to almost 6 during oxidation of the Fe(II) system (Table 1), suggesting that the primary clusters are growing in two dimensions, forming chloride GR (28) (Figure 5). In contrast,  $N_{\text{FeE}}$  decreases from 3.8 to  $\sim 2.11$  during oxidation of the Fe(II)–As(III) system, suggesting a decrease of the size of the clusters (Figure 5, Table 2). Even if it is difficult to estimate the size using XAFS data, in the case of the Fe(II)–As(III) system, the individual Fe clusters appear to be composed of fewer than 20 Fe octahedra, whereas chloride green rust is formed in the Fe(II) system. X-ray diffraction analysis conducted on precipitate from the Fe(II)–As(III) system indicates that the particles were amorphous (not shown), confirming the EXAFS results. The final oxidation products of the Fe(II) system were not analyzed, but it seems reasonable to assume that the evolution of chloride GR leads to the formation of a mixture of lepidocrocite, goethite, and/or akaganeite, as previously suggested (44, 45).

In summary, the experiments indicate that As(III) hinders the formation of GR at the onset of Fe(II) oxidation and that As(III)–Fe(II) interactions result in the formation of amorphous particles composed of nanosized clusters. The small clusters might be more sensitive to oxidation, which could explain the effect of As(III) on Fe(II) oxidation. Das and Anand (46) have also shown that the presence of As(III) reduces Fe precipitation by decreasing the particle size. The same study demonstrated the formation of amorphous As–Fe precipitates under conditions that could have resulted in the formation of magnetite.

**Implications of Fe(II)–As(III) Interactions for Natural Waters.** Results from the present study must be extrapolated to natural systems with care because the As/Fe ratio of 1 in the experiments was rather high. Comparable As/Fe ratios



### Legend

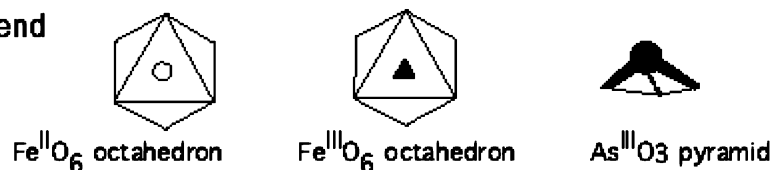


**FIGURE 5.** Possible structural evolution of the Fe(II) and Fe(III)–As(III) systems through oxidation constructed on the basis of the structural parameters derived from Fe and As EXAFS analysis (listed in Tables 1 and 2). The average numbers of Fe neighbors around Fe and As and of As neighbors around Fe [in the case of the Fe(II)–As(III) system] were calculated according a procedure described by Rose et al. (40) and detailed in the Supporting Information. The clusters are proposed to illustrate the size evolution of the particles or the size of subunits constituting larger particles.

are typically encountered in highly contaminated systems (e.g., mining areas). Morin et al. (47), for example, analyzed As/Fe ratios between 0.5 and 0.72 in contaminated sediment. Nevertheless, elevated As/Fe ratios of up to 0.5 have also been observed in various parts of the Bangladesh (48). The analysis of the data from the British Geological Survey (49) (3534 bore holes from 61 of the 64 districts of Bangladesh) indicates that more than 5% of the wells containing more than 0.1 mg/L of Fe exhibit an As/Fe molar ratio higher than 0.1. The highest ratio detected was 0.83.

The very strong and well-documented affinity of As species for iron oxyhydroxides is the basis for the passive removal of As from contaminated groundwaters containing dissolved Fe(II). Aeration of such water results in the formation of iron(III) oxyhydroxides and adsorption and/or co-precipitation of As (17, 50, 51). Previous studies have consistently shown that As removal is limited by the interactions of solutes, mainly P and Si, competing with iron in the form of Fe(III) (17, 50, 51). The negative impact of As on the size of Fe particles on As removal because of an increase in settling

time has also been noted previously (52). The present study suggests that competing ions might already play a role when iron is still in the form of Fe(II) and demonstrates that As(III) indeed limits the size of Fe particles formed during oxidation.

The hindrance of Fe(III) polymerization during oxidation can also strongly impact the mobility of As during seasonal redox cycles. Indeed, small clusters of amorphous particles are more sensitive to the redox cycle and can be easily dissolved during reductive seasonal events in groundwater sediments (53, 54). Therefore, such As(III)–Fe(III) nano-clusters might correspond to a relatively mobile As form during reductive dissolution of Fe phases. As a result, the relatively strong affinity between As(III) and Fe leads to an unpredicted mobile As–Fe species during redox cycles. Our observations should also help correct the widely believed notion that the reduction of Fe(III) phases onto which As(III) is adsorbed and/or coprecipitated necessarily leads to the desorption of As(III).

### Acknowledgments

This research was funded by the ACI “Eau et Environnement” from the French ministry of research. The LURE (Laboratoire pour l’Utilisation du Rayonnement Electromagnétique, Orsay, France) is acknowledged for the provision of beam time.

### Supporting Information Available

Evolution of  $E_h$  as a function of time during the oxidation of Fe(II) and coprecipitated Fe(II)–As(III) with ambient air, XANES spectra of Fe(II) systems exhibiting different structures, and calculation of the average number of Fe neighbors as a function of Fe(OH)<sub>2</sub> layer size. This material is available free of charge via the Internet at <http://pubs.acs.org>.

### Literature Cited

- (1) Korte, N. E.; Fernando, Q. A review of arsenic(III) in groundwater. *Crit. Rev. Environ. Control.* **1991**, *21*, 1–39.
- (2) Pierce, M. L.; Moore, C. B. Adsorption of arsenite and arsenate on amorphous iron hydroxide. *Water Res.* **1982**, *16*, 1247–1253.
- (3) Inskeep, W. P.; McDermott, T. R.; Fendorf, S. E. Arsenic(V)/(III) cycling in soils and natural waters: Chemical and microbiological processes. In *Environmental Chemistry of Arsenic*; Frankenberger, W. F., Jr.; Macy, J. M., Eds.; Marcel Dekker: New York, 2001; pp 183–215.
- (4) Hug, S. J.; Canonica, L.; Wegelin, M.; Gechter, D.; Von Gunten, U. Solar oxidation and removal of arsenic at circumneutral pH in iron containing waters. *Environ. Sci. Technol.* **2001**, *35* (10), 2114–2121.
- (5) British Geological Survey and Department of Public Health Engineering. Arsenic contamination of groundwater in Bangladesh. In *British Geological Survey Technical Report WC/00/19*; Kinniburgh, D. G., Smedley, P. L., Eds.; British Geological Survey: Keyworth, U.K., 2001; Vol. 2 (<http://www.bgs.ac.uk/arsenic/Bangladesh>).
- (6) Zobrist, J.; Dowdle, P. R.; Davis, J. A.; Oremland, R. S. Mobilization of arsenite by dissimilatory reduction of adsorbed arsenate. *Environ. Sci. Technol.* **2000**, *22*, 4747–4753.
- (7) Savage, K. S.; Tingle, T. N.; O’Day, P. A.; Waychunas, G. A.; Bird, D. K. Arsenic speciation in pyrite and secondary weathering phases, Mother Lode Gold District, Tuolumne County, California. *Appl. Geochem.* **2000**, *15* (8), 1219–1244.
- (8) Waychunas, G. A.; Rea, B. A.; Fuller, C. C.; Davis, J. A. Surface chemistry of ferrihydrite. 1. EXAFS studies of the geometry of coprecipitated and adsorbed arsenate. *Geochim. Cosmochim. Acta.* **1993**, *57*, 2251–2269.
- (9) Manceau, A. The mechanism of anion adsorption on iron oxides—Evidence for the bonding of arsenate tetrahedra on free Fe(O,OH)(6) edges. *Geochim. Cosmochim. Acta* **1995**, *59* (17), 3647–3653.
- (10) Fendorf, S. Eick, M. J., Grossl, P.; Sparks, D. L. Arsenate and chromate retention mechanisms on goethite. 1. Surface structure. *Environ. Sci. Technol.* **1997**, *31* (2), 315–320.
- (11) Farquhar, M. L.; Charnock, J. M.; Livens, F. R.; Vaughan, D. J. Mechanisms of arsenic uptake from aqueous solution by interaction with goethite, lepidocrocite, mackinawite, and

- pyrite: An X-ray absorption spectroscopy study. *Environ. Sci. Technol.* **2002**, *36*, 1757–1762.
- (12) Thorat, S.; Rose, J.; Garnier, J. M.; van Geen, A.; Masion, A.; Proux, O.; Hazemann, J. L.; Bottero, J. Y. Complex as speciation in Bangladesh groundwater: An EXAFS study. *Geochim. Cosmochim. Acta*, manuscript in preparation.
- (13) Randall, S. R.; Sherman, D. M.; Ragnarsdottir, K. V. Sorption of As(V) on green rust (Fe<sub>4</sub><sup>III</sup>Fe<sub>2</sub><sup>III</sup>(OH)<sub>12</sub>SO<sub>4</sub>·3H<sub>2</sub>O) and lepidocrocite (γ-FeOOH): Surface complexes from EXAFS spectroscopy. *Geochim. Cosmochim. Acta* **2001**, *65* (7), 1015–1023.
- (14) Manning, B. A.; Fendorf, S. E.; Goldberg, S. Surface structures and stability of arsenic(III) on goethite: Spectroscopic evidence for inner-sphere complexes. *Environ. Sci. Technol.* **1998**, *32*, 2383–2388.
- (15) Horneman, A.; van Geen, A.; Kent, D. V.; Mathe, P. E.; Zheng, Y.; Dhar, R. K.; O’Connell, S.; Hoque, M. A.; Aziz, Z.; Shamsudduha, M.; Seddique, A. A.; Ahmed, K. M. Decoupling of As and Fe release to Bangladesh groundwater under reducing conditions. Part 1: Evidence from sediment profiles. *Geochim. Cosmochim. Acta* **2004**, *68* (17), 3459–3473.
- (16) Dixit, S.; Hering, J. G. Comparison of arsenic(V) and arsenic(III) sorption onto iron oxide minerals: Implications for arsenic mobility. *Environ. Sci. Technol.* **2003**, *37* (18), 4182–4189.
- (17) Meng, X. G.; Bang, S. B.; Korfiatis, G. P. Effects of silicate, sulfate, and carbonate on arsenic removal by ferric chloride. *Water Res.* **2000**, *34*, 1255–1261.
- (18) Baes, C. F.; Mesmer, R. E. *The Hydrolysis of Cations*; John Wiley & Sons: New York, 1974.
- (19) Doelsch, E.; Rose, J.; Masion, A.; Bottero, J. Y.; Nahon, D.; Bertsch, P. M. Speciation and crystal chemistry of iron(III) chloride hydrolyzed in the presence of SiO<sub>4</sub> ligands. 1. An Fe K-edge EXAFS study. *Langmuir* **2000**, *16* (10), 4726–4731.
- (20) Mickalowicz, A. “EXAFS pour le MAC”: A new version of an EXAFS data analysis code for the Macintosh. *J. Phys. IV* **1997**, *C2*, 235.
- (21) Manceau, A.; Calas, G. Nickel-bearing clay minerals. 2. Intracrystalline distribution of nickel—An X-ray absorption study. *Clay Mineral.* **1986**, *21*, 341–360.
- (22) Manceau, A. Structure of Mn and Fe oxides and oxyhydroxides—A topological approach by EXAFS. *Phys. Chem. Min.* **1988**, *15*, 283–295.
- (23) Ankudinov, A. L.; Rehr, J. J. Relativistic calculations of spin-dependent X-ray absorption spectra. *Phys. Rev. B* **1997**, *56*, R1712.
- (24) Galois, L.; Calas, G.; Arrio, M. A. High-resolution XANES spectra of iron in minerals and glasses: Structural information from the preedge region. *Chem. Geol.* **2001**, *174*, 307–319.
- (25) Petit, P. E.; Farges, F.; Wilke, M.; Solé, V. A. Determination of the iron oxidation state in Earth materials using XANES preedge information. *J. Synchrotron Radiat.* **2001**, *8*, 952–954.
- (26) Giulì, G.; Pratesi, G.; Cipriani, C.; Paris, E. Iron local structure in tektites and impact glasses by extended X-ray absorption fine structure and high-resolution X-ray absorption near-edge structure spectroscopy. *Geochim. Cosmochim. Acta* **2002**, *66* (24), 4347–4353.
- (27) Combes, J.-M.; Manceau, A.; Calas, G.; Bottero, J.-Y. Formation of Ferric Oxides from Aqueous Solutions—A Polyhedral Approach by X-ray Absorption Spectroscopy. 1. Hydrolysis and Formation of Ferric Gels. *Geochim. Cosmochim. Acta* **1989**, *53* (3), 583–594.
- (28) Manceau, A.; Combes, J. M. Structure of Mn and Fe oxides and oxyhydroxides: A topological approach by EXAFS. *Phys. Chem. Min.* **1988**, *15*, 283–295.
- (29) Simon, L.; François, M.; Refait, P.; Renaudin, G.; Lelaurain, M.; Génin, J.-M. R. Structure of the Fe(II–III) layered double hydroxysulphate green rust two from Rietveld analysis. *Solid State Sci.* **2003**, *5*, 327–334.
- (30) Doelsch, E.; Rose, J.; Masion, A.; Bottero, J. Y.; Nahon, D.; Bertsch, P. M. Hydrolysis of Iron(II) Chloride in Reducing Conditions and Influence of SiO<sub>4</sub> Ligands. *Langmuir* **2002**, *18*, 4292–4299.
- (31) Sherman, D. M.; Randall, S. R. Surface complexation of arsenic(V) to iron(III) (hydr)oxides: Structural mechanism from ab initio molecular geometries and EXAFS spectroscopy. *Geochim. Cosmochim. Acta* **2003**, *67* (22), 4223–4230.
- (32) Bottero, J.; Manceau, A.; Villieras, F.; Tchoubar, D. Structure and mechanisms of formation of FeOOH(Cl) Polymers. *Langmuir* **1994**, *10* (1), 316–319.
- (33) Vilgé-Ritter, A.; Rose, J.; Masion, A.; Bottero, J. Y.; Lainé, J. M. Chemistry and structure of aggregates formed with Fe salts and natural organic matter. *Colloids Surf. A: Physicochem. Eng. Aspects* **1999**, *147*, 297–308.

- (34) Rose, J.; Manceau, A.; Masion, A.; Bottero, J. Y. Structure and mechanisms of formation of FeOOH(NO<sub>3</sub>) oligomers at the early stages of hydrolysis. *Langmuir* **1997**, *13*, 3240–3246.
- (35) Rose, J.; Vilgé, A.; Olivie-Lauquet, G.; Masion, A.; Frechou, C.; Bottero, J. Y. Iron speciation in natural organic matter colloids. *Colloids Surf. A: Physicochem. Eng. Aspects* **1998**, *136*, 11–19.
- (36) Refait, P.; Abdelmoula, M.; Trolard, F.; Génin, J.-M. R.; Ehrhardt, J.-K.; Bourrié, G. Mossbauer and XAS study of a green rust mineral; the partial substitution of Fe<sup>2+</sup> by Mg<sup>2+</sup>. *Am. Mineral.* **2001**, *86*, 731–739.
- (37) Pokrovski, G. S.; Schott, J.; Farges, F.; Hazemann J.-L. Iron(III)–silica interactions in aqueous solution: Insights from X-ray absorption fine structure spectroscopy. *Geochim. Cosmochim. Acta* **2003**, *67* (19), 3559–3573.
- (38) O'Day, P. A.; Rivera, N., Jr.; Root, R.; Carroll, S. A. X-ray absorption spectroscopic study of Fe reference compounds for the analysis of natural sediments. *Am. Mineral.* **2004**, *89*, 572–585.
- (39) Benali, O.; Abdelmoula, M.; Refait, Ph.; Génin, J.-M. R. Effect of orthophosphate on the oxidation products of Fe(II)–Fe(III) hydroxycarbonate: The transformation of green rust to ferrihydrite. *Geochim. Cosmochim. Acta* **2001**, *65* (5), 1715–1726.
- (40) Rose, J.; Cortalezzi-Fidalgo, M. M.; Moustier, S.; Magnetto, C.; Jones, C. D.; Barron, A. R.; Wiesner, M. R.; Bottero, J. Y. Synthesis and characterisation of carboxylate–FeOOH nanoparticles (Ferroxane) and Ferroxane-derived ceramics. *Chem. Mater.* **2002**, *14*, 621–628.
- (41) Masion, A.; Rose, J.; Bottero, J. Y.; Tchoubar, D.; Elmerich, P. Nucleation and growth mechanisms of Fe oxyhydroxides in the presence of PO<sub>4</sub> ions. 3. Speciation of Fe by small-angle X-ray scattering. *Langmuir* **1997**, *13*, 3882–3885.
- (42) Masion, A.; Rose, J.; Bottero, J. Y.; Tchoubar, D.; Garcia, F. Nucleation and growth mechanisms of Fe oxyhydroxides in the presence of PO<sub>4</sub> ions. 4. Structure of the aggregates. *Langmuir* **1997**, *13*, 3886–3889.
- (43) Jolivet, J.-P. *Metal Oxide Chemistry and Synthesis: From Solution to Solid State*; John Wiley & Sons: New York, 2000.
- (44) Schwertmann, U.; Fechter, H. The formation of green rust and its transformation to lepidocrocite. *Clay Mineral.* **1994**, *29*, 87–92.
- (45) Refait, P.; Génin, J. M. R. The oxidation of ferrous hydroxide in chloride-containing aqueous media and pourbaix diagrams of green rust one. *Corrosion Sci.* **1993**, *34*, 797–819.
- (46) Das, R. P.; Anand, S. Precipitation of arsenic in the Fe(II)–NH<sub>3</sub>–(NH<sub>4</sub>)<sub>2</sub>–SO<sub>4</sub>–O<sub>2</sub> system. *Hydrometallurgy* **1999**, *53*, 267–277.
- (47) Morin, G.; Juillot, F.; Casiot, C.; Bruneel, O.; Personne, J.-C.; Elbaz-Poulichet, F.; Leblanc, M.; Ildefonse, P.; Calas, G. Bacterial Formation of Tooeleite and Mixed Arsenic(III) or Arsenic(V)–Iron(III) Gels in the Carnoules's Acid Mine Drainage, France. A XANES, XRD, and SEM Study. *Environ. Sci. Technol.* **2003**, *37* (9), 1705–1712.
- (48) Thoral, S. Ph.D. Thesis. Univeristy Paul Cezanne, Aix en Provence, France ([www.cerege.fr](http://www.cerege.fr)).
- (49) British Geological Survey. The groundwater arsenic problem in Bangladesh (Phase 2), DPHE/BGS National Hydrochemical Survey. British Geological Survey: Keyworth, U.K. (<http://www.bgs.ac.uk/arsenic/bangladesh/datadownload.htm>.)
- (50) Meng, X. G.; Korfiatis, G. P.; Bang, S. B.; Bang, K. W. Combined effects of anions on arsenic removal by iron hydroxides. *Toxicol. Lett.* **2002**, *133*, 103–111.
- (51) Meng, X. G.; Korfiatis, G. P.; Christodoulatos, C.; Bang, S. Treatment of arsenic in Bangladesh well water using a household coprecipitation and filtration system. *Water Res.* **2001**, *35* (12), 2805–2810.
- (52) Daus, B.; Mattusch, J.; Paschke, A.; Wennrich, R.; Weiss, H. Kinetics of the arsenite oxidation in seepage water from a tin mill tailings pond. *Talanta* **2000**, *51*, 1087–1095.
- (53) Cheng, Z.; van Geen, A.; Jing, C.; Meng, X.; Seddique, A. A.; Ahmed, K. M. Performance of a household-level arsenic removal system during 4-month deployments in Bangladesh. *Environ. Sci. Technol.* **2004**, *38*, 3442–3448.
- (54) Cheng, Z.; van Geen, A.; Seddique, A. A.; Ahmed, K. M. Limited temporal variability of arsenic concentration in 20 wells monitored for 3 years in Araihaazar, Bangladesh. *Environ. Sci. Technol.* **2005**, *39*, 4759–4766.

Received for review December 22, 2004. Revised manuscript received September 5, 2005. Accepted September 12, 2005.

ES047970X